Direct numerical simulation on the particle flow in the wake of circular cylinder*

YAO Jun, JI Feng, LIU Lan, FAN Jianren** and CEN Kefa

(Institute of Thermal Power Engineering, Zhejiang University, Hangzhou 310027, China)

Received November 11, 2002; revised December 25, 2002

Abstract The spectral-element approach is used to simulate the gas-solid two-phase flow behind of the circular cylinder. Based on the method of a high accuracy calculation for the gas phase flow, the particle dynamic field is put into practice. Two key influence factors, Stokes number and Reynolds number, are investigated. The simulation results give a clear pattern of the physical characteristics of gas-particle flow. Due to the construction properties of the eddies in the wake of the circular cylinder, the suction is the main dispersion mechanism of particles near to the centric axis. This effect can make the small particle sucted to the near wake of the circular cylinder. The particle dispersion is also induced by the pressure gradient which is caused by the strong velocity gradient of gas phase.

Keywords: direct numerical simulation, gas-particle two-phase flow, circular cylinder.

The problems related with the wakes behind of the bluff bodies and in particular of circular cylinders are the hot points to the scientists and engineers[1,2]. The transport of particles passing through the circular cylinder wake is a universal phenomenon found in many natural and technological flow systems. Therefore, the research on the mechanism of particle dispersion in such flows has not only theoretical significance but also engineering practical significance.

A lot of research work in this field has been done, and some valuable results have been obtained[3~5]. However, there are still some unresolved problems. For example, the calculation results and experimental data have a big discrepancy due to the low accuracy of calculating methods used. Furthermore, the coherent structure of the particle dispersion in the wake of the circular cylinder has never been characterized. In recent years, the different high accuracy algorithm is used to simulate the flow around a circular cylinder. There are many articles on the circular cylinder flow with application of the high accuracy algorithm. But few of them are concerned about the particle flow. This paper uses spectral-element method to simulate the gas-solid two-phase flow behind the circular cylinder. Based on the high accuracy calculation of the gas flow, an investigation of particle dispersion patterns in temporal cylinder wake at $Re \leqslant 175$ would be made.

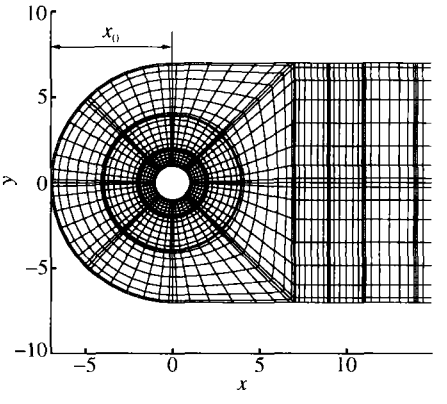

Fig. 1. A sketch of the computational domain.

1 Mathematical model and algorithm

The computational mesh is shown in Fig. 1. The computational time step is taken as 0.01.

1.1 Gas-phase governing equations

The N-S equation and mass conservation equation of incompressible viscous fluid flow are normalized as follows:

$$\frac{\partial \boldsymbol{V}}{\partial t} = -\nabla p + \frac{1}{Re}\boldsymbol{L}(\boldsymbol{V}) + \boldsymbol{N}(\boldsymbol{V}) \quad \text{in } \Omega, \quad (1)$$

$$\nabla \cdot \boldsymbol{V} = \boldsymbol{0} \quad \text{in } \Omega, \quad (2)$$

where $\boldsymbol{V}$ is the velocity, p the pressure (density $\rho = 1$); Re, the Reynolds number, defined as $Re = Ud/\nu$, in which U is the uniform stream velocity, d the characteristic length, and ν the kinematic viscosity.

* Supported by the National Natural Science Foundation of China (Grant Nos. 50236030 and 50076038)

** To whom correspondence should be addressed. E-mail: fanjr@public.hz.zj.cn

Its initial condition and boundary condition depend on the practical circumstances. Linear dispersion operator and nonlinear convection operator are:

$$\boldsymbol{L}(\boldsymbol{V}) = \nabla^2 \boldsymbol{V},$$

$$\boldsymbol{N}(\boldsymbol{V}) = -\frac{1}{2}[\boldsymbol{V}\cdot\nabla\boldsymbol{V} + \nabla\cdot(\boldsymbol{V}\boldsymbol{V})], \quad (3)$$

represented in the oblique symmetric form to reduce the anti-aliased error.

1.2 Algorithm

N-S equations are discretized by mixed explicit/implicit operator splitting rules[6], which can be implemented in three steps:

$$\frac{\hat{\boldsymbol{V}} - \sum_{q=0}^{J_e-1}\alpha_q \boldsymbol{V}^{n-q}}{\Delta t} = \sum_{q=0}^{J_i-1}\beta_q \boldsymbol{N}(\boldsymbol{V}^{n-q}), \quad (4)$$

$$\frac{\tilde{\boldsymbol{V}} - \boldsymbol{V}}{\Delta t} = -\nabla \bar{p}^{n+1}, \quad (5)$$

$$\frac{\gamma_0 \boldsymbol{V}^{n+1} - \tilde{\boldsymbol{V}}}{\Delta t} = Re^{-1}\nabla^2 \boldsymbol{V}^{n+1}, \quad (6)$$

where $\hat{\boldsymbol{V}}$, $\tilde{\boldsymbol{V}}$ are intermediate velocity fields defined in Eqs. (4) and (5), J_e and J_i are the parameters characterizing the accuracy of the overall scheme, α_q, β_q, γ_0 are the suited weight-coefficients. In the present research, the process of time-discretization is implemented by the third order with the parameters listed in Table 1.

Table 1. Values of weight-coefficients used

γ_0	α_0	α_1	α_2	β_0	β_1	β_2
11/6	3	-3/2	1/3	3	-3	1

The special discretization is processed by the spectral-element method[7,8]. The computational domain is discretized into a series of quadrangular elements in two dimensions, which are mapped isoparametrically to canonical squares. Grid nodes of the physical plane can be generated by the following method: points on each side of the quadrangular elements are expressed through Chebyshev collocation points. For the computational boundary, it is usually given; while the inner boundary depends on the accuracy. In the computational plane, the primary function is the direct product of two one-dimensional N-order Lagrange interpolation polynomials. 1-D Lagrangian interplant is expressed as the following:

$$h_m(z) = \mu_{mn} T_n(z),$$

$$\mu_{mn} = \frac{2}{N}\frac{1}{\bar{C}_m \bar{C}_n} T_n(z_m), \quad (7)$$

it satisfies

$$h_m(z_n) = \delta_{mn},$$

where z_n is Gauss-Lobatto-Chebyshev collocation points, T_n is Chebyshev polynomial:

$$z_n = -\cos\frac{\pi n}{N}. \quad (8)$$

The problem to be solved is usually at the unsteady flow in the specified geometry domain. As the coefficient matrix is only related to the geometric parameters, it only needs to be calculated once.

In the present research, the equations degree of freedom is reduced remarkably by applying standard matrix condensation. Inner value of the element can be calculated after having calculated the boundary ones.

The inflow boundaries with an initial condition are as follows:

$u = 1$, $v = 0$ and $\partial u/\partial n = 0$, $v = 0$. And non-reflecting boundary condition is employed to the outflow.

1.3 Particle motion equation

For simplifying analysis, assumptions are made as follows: (i) All particles are rigid spheres with the same diameter and density; (ii) the density of particles is much larger than that of the gas; (iii) particle-particle interactions are neglected; (iv) pressure gradient, virtual mass and Basset force of particles are neglected.

The non-dimensional equation of motion of a particle is expressed as:

$$\frac{\mathrm{d}\boldsymbol{V}}{\mathrm{d}t} = f/St(\boldsymbol{U} - \boldsymbol{V}) + \hat{g}, \quad (9)$$

where $\boldsymbol{V}$ is the particle velocity, $\boldsymbol{U}$ is the fluid velocity at that particle position and f is a modification factor for the Stokes drag coefficient, which is described by[9] $f_p = 1 + 0.15\, Re_p^{0.687}$, with $Re_p = |\boldsymbol{U} - \boldsymbol{V}| d_p/\nu$, St named as Stokes number for a particle, defined as: $St = (\rho_p d_p^2/18\mu)/(R/\boldsymbol{U}_0)$; non-dimensional acceleration of gravity is $\hat{g} = 9.8R/\boldsymbol{U}_0^2$.

1.4 Particle-wall collision model

Grant and Tabakoff[10] gave the expression of particle-wall collision by practical experiments. The change in particle momentum due to impact is found to be mainly a function of the particle impact velocity

and its incidence angle.

$$\frac{V_{n_2}}{V_{n_1}} = 1.0 - 0.4159\beta_1 - 0.4994\beta_1^2 + 0.292\beta_1^3, \quad (10)$$

$$\frac{V_{t_2}}{V_{t_1}} = 1.0 - 2.12\beta_1 + 3.0775\beta_1^2 - 1.1\beta_1^3, \quad (11)$$

where V_n and V_t represent the particle velocity impact components normal and tangential to the wall, respectively. Subscripts 1 and 2 refer to the conditions before and after impact, respectively. In the above equations, β_1(in radians) is the angle between the incident velocity and the tangent to the surface.

2 Numerical results and discussion

2.1 Flow field analysis

The drag coefficient C_d is calculated by every 5 steps from $Re = 25$ to $Re = 60$, and the computational results are compared with the experiment results[11] (Fig. 2). It can be seen that the average error between the numerical results and experimental data is about 4%.

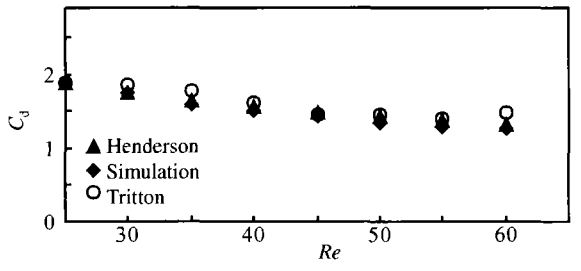

Fig. 2. Mean drag coefficient versus Reynolds number.

2.2 Particle flow analysis

As the exact gas flow field was determined at each time, the particle motion may be done. Particle flow updates instantaneously to follow the change of gas flow. This can reflect the particle motion exactly and show the characteristics of particle motion in the vortex. The computational time step is 0.01, and the overall physical time is 100 unit time (10000 steps).

Fig. 3 describes the particle dispersion characteristic in center of the wake varying with time. It can be seen clearly that the flow patterns and hydrodynamics of small particles have a distinct vortex structure with obvious stretch. Simulation results show that the small particles can follow the gas flow, mixed with vortex sufficiently and entrained into vortex core. With the time continuing, a vortex street is formed behind the circular cylinder. In the sheet between two adjacent vortex structures with opposite sign, the particle motion following gas flow manifests a mushroom characteristic.

In order to study the physical properties of particle motion in the vortex for the particles flow passing the circular cylinder, the simulations of different cases were made according to the particle diffusion effects. The effects of particle diameter or Stokes number and Reynolds number on the particle diffusion were considered. The three groups of particle diameter corresponding to the Stokes number of 0.1, 1.0 and the Reynolds number of 100 and 175 were calculated.

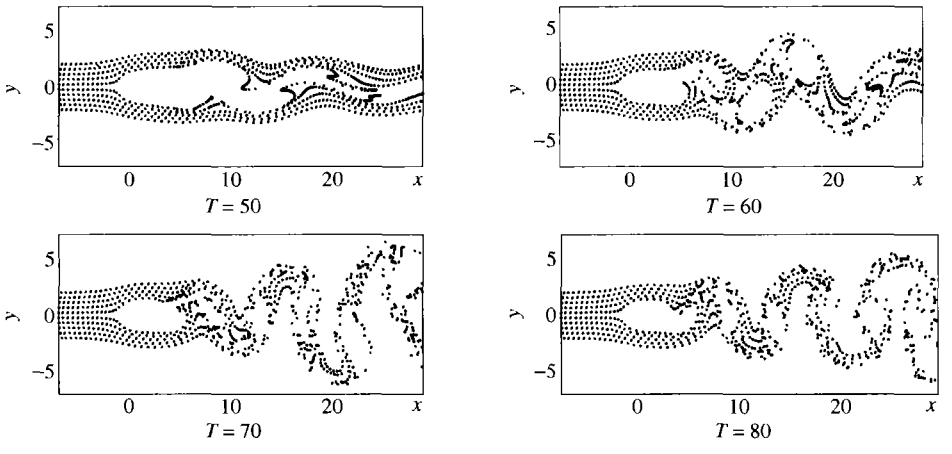

Fig. 3. Time-dependent distribution of particles at $Re = 100$, $St = 0.1$.

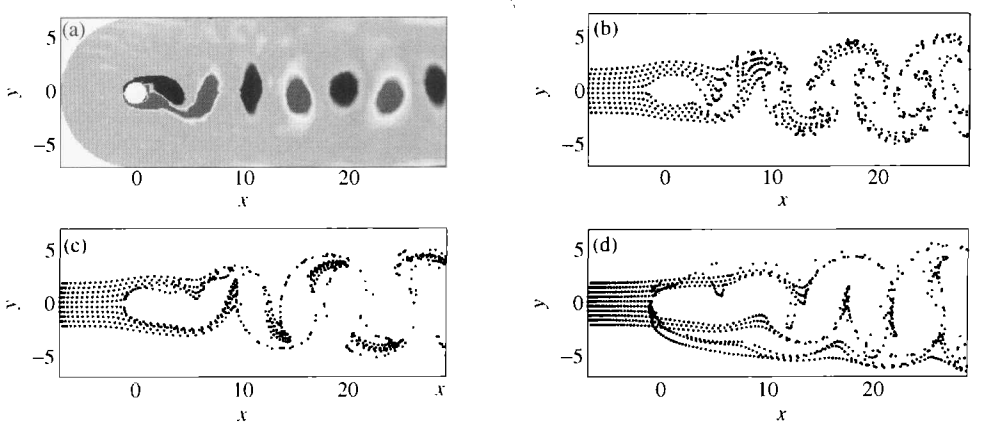

Fig. 4. Gas flow and particle flow with different Stokes number at $Re = 100$, $t = 100$. a) gas flow vorticity field; b), c), d) distribution of particles at $St = 0.1$, 1, 10 respectively.

Fig. 4 shows the gas and particle motion with different Stokes number at the Reynolds number of 100. The inlet width is from −2 to 2. According to the figure, it can be easily seen that the particle flow is similar to the gas flow when St equals 0.1. That is to say, it is obvious that particles follow the gas flow and they do not collide with the front face of the cylinder when the particle size is small. And part of the particles have got into the vortex core. When St equals 1, especially 10, almost no particle would get into the core basically because of the inertial effect of large particles. The ability of particle following gas phase decreases as Stokes number increases, and the influence of gas flow decreases slowly. Furthermore, the particles begin to collide with the front face of the cylinder, especially violently at $St = 10$. The collision particles offset the trajectories of most particles, it seems that their motion is chaotic.

When Re equals 175, the perturbation is stronger than that of 100. The particle flow dynamic characteristics are changed. For examples, when both of Stokes numbers are 0.1, the irregularities of particle flow vortex structure increase due to the stronger perturbation. As the Stokes number increases, the change trend of particle flow is similar for different Reynolds numbers. All of them have the characteristics that the follow becomes weakened and the collision possibilities increased.

2.3 Factors affecting particle dispersion

Two key factors, particle Stokes number and Reynolds number of gas phase are considered.

2.3.1 Particle Stokes number Particle Stokes number is a primary factor in determining particle dispersion. For small Stokes numbers (small particles), the particles should closely follow the fluid element, and the particle /fluid dispersion ratio should be approximately unity. On the contrary, for large Stokes numbers, the fluid element motion should have little effect on the particles, and the particle/fluid dispersion ratio should approach zero. However, particles having moderate Stokes number might be dispersed significantly faster than the fluid element motion due to the centrifugal effects created by the organized vortex structures.

Instantaneous particle dispersion (Fig. 3) demonstrates that the small particles do fill in the inner regions of the vortices. To make a clear contrast, vertical dispersion function is introduced[12]

$$D_y(t) = \left\{ \sum_{i=1}^{n_t} (Y_i(t) - Y_m(t))^2 / n_t \right\}^{1/2}, \tag{12}$$

where n_t is the total particle numbers in the computational domain at the time t, $Y_i(t)$ is the ith particle instantaneous vertical displacement. $Y_m(t)$ is the mean vertical displacement of total particles at that time. This function reflects the degree of particle dispersions.

As particle Stokes numbers increase at order unity ($St = 1$), the aerodynamic response time is at the same order of the characteristic vortex time. As a result, particles tend to accumulate at the periphery of vortex structure giving a good visualization of the large vortices structures, manifested by Fig. 4(b), (c).

Particle dispersion function in vertical direction is quantitatively and instantaneously plotted in Fig. 5.

It is observed that particle dispersion function decreases with the increasing particle Stokes number. For the circular cylinder wake, two symmetrical vortices with opposite sign are separately and alternately generated. They are convected and diffused away from the cylinder but no vortex pairing interaction happens. The mechanism for the particle dispersion in circular cylinder wake mainly depends on the repulsion force associated with the vortex sheet regions between two adjacent vortex structures with opposite sign, which is named stretching process.

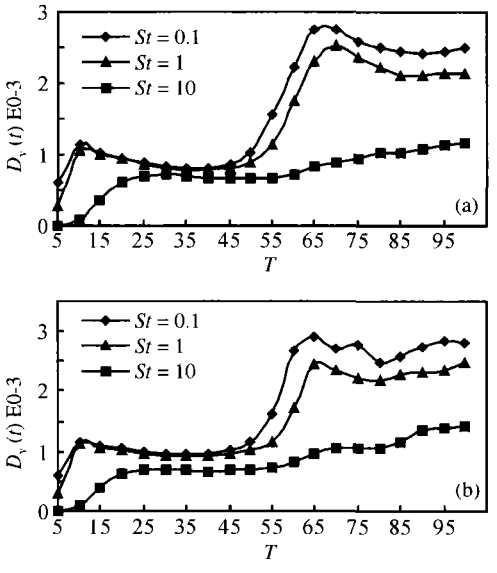

Fig. 5. Time-dependent particle dispersion in the vertical direction. (a) $Re = 100$; (b) $Re = 175$.

2.3.2 Gas Reynolds number Based on the physical character of cylinder wake[1,2], it is known that the amplitudes of the oscillations for the wake velocity, drag and lift coefficients increase as the Reynolds number increases. The higher the Reynolds numbers, the more violent the wake shedding behind a circular cylinder. Apparently, the Reynolds number of gas phase does have effect on particle dispersion. It shows that the extent of particles merging interaction with vortex structure is increased as the Reynolds number increases, which results in particles well distributed in the global region at higher Reynolds numbers.

The fact that the well-distributed particles increases with increase of Reynolds numbers can be examined more clearly in two physical processes. First, with Reynolds number increasing, vortex structures spawned at higher frequency causes particles well-distributed in the center region near $X = 0$ line. Second, with Reynolds number increasing, a large-scale structure of cylinder wake is stretched at higher amplitudes and it makes particles move as broadly as possible with the vortex structure, which mainly contributes to the distribution of particles in the outter region. The effect of Reynolds numbers on particle dispersion is demonstrated in Fig. 6.

In summary, it can be concluded that the higher the Reynolds number is, the more even the particle distribution is. The dynamical mechanism of such a phenomenon can be explained by the following facts. Because the circular cylinder wake is typically composed of an alternating arrangement of opposite sign vortex structures that convect downstream from the near wake region, the sheet between two adjacent vortex structures with opposite sign generates a great pressure gradient, which results in a large repulsion. When particles with small Stokes numbers approach the sheet, they would be caught firmly by such a strong repulsion and thrown into the region close to cylinder back or even collide with the cylinder. Besides, turbulent flow with a small Reynolds number cannot produce sufficient repulsion to force particles moving towards the circular cylinder (Fig. 3, $Re = 100$).

It seems that the amplitude and frequency of particle dispersion increase when Reynolds number increases.

3 Conclusions

Simulation results give the coherent structure of particle motion at the back of circular cylinder.

First, particle Stokes number (size) is a primary factor in determining particle dispersion. The smaller the particle Stokes number the more even particle dispersion (Fig. 6).

Second, Reynolds number is another factor affecting particle dispersion. It can be summarized that the higher the Reynolds number the more even the particle distribution. Particularly, it is found that the sheet between two adjacent vortex structures with opposite sign possesses a great pressure gradient resulting in a large repulsion in it. Particle dispersion mechanism near the center axis of the flow is mainly determined by this suction.

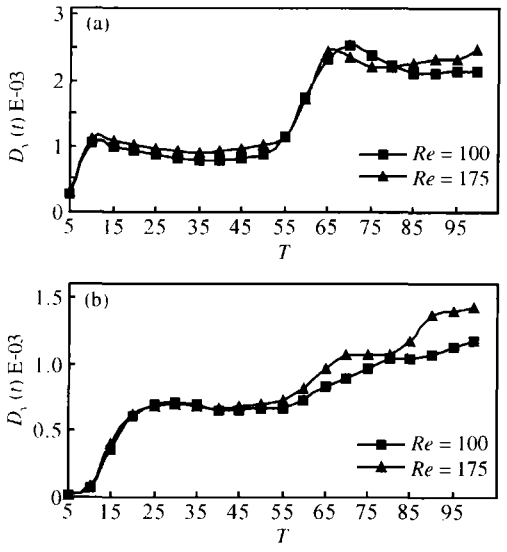

Fig. 6. Distribution of particles at different Reynolds number. (a) $St = 1$; (b) $St = 10$.

References

1 Williamson, C. H. K. Vortex dynamics in the wake of a cylinder wake. Ann. Rev. Fluid Mech., 1996, 28: 477.

2 Perillon, H. et al. Physical analysis of the transition to turbulence in the wake of a circular cylinder by three-dimensional Navier-Stokes simulation. J. Fluid Mech., 1998, 365: 23.

3 Morsi, S. A. et al. An investigation of particle trajectories in two-phase flow systems. J. Fluid Mech., 1972, 55(2): 193.

4 Michael, D. H. et al. Particle collision efficiencies for a sphere. J. Fluid Mech., 1969, 37(3): 565.

5 Healy, J. V. Perturbed two-phase cylindrical type flows. Phys. Fluids, 1970, 13(3): 551.

6 Karniadakis, G. E. et al. High-order splitting methods for the incompressible Navier-Stokes equations. J. Comput. Phys., 1991, 97: 414.

7 Patera, A. T. A spectral element method for fluid dynamics: laminar flow in a channel expansion. Journal of Computational Physics, 1984, 54: 468.

8 Korczak, K. Z. et al. An isoparametric spectral element method for solution of the Navier-Stokes equations in complex geometry. Journal of Computational Physics, 1986, 62: 361.

9 Sommerfeld, M. et al. Recent advances in the numerical simulation of pneumatic conveying through tube systems. In: Computational Methods in Applied Sciences (ed. Ch. Hirsch), Amsterdam: Elsevier Science, 1992, 201.

10 Grant, G. at al. Erosion prediction in turbomachinery resulting from environ-mental solid particles. J. of Aircraft, 1975, 12: 471.

11 Henderson, R. D. Details of the drag curve near the onset of vortex shedding. Phys. Fluids, 1995, 7(9): 2102.

12 Ling, W. et al. Direct numerical simulation of a three-dimensional temporal mixing layer with particle dispersion. J. Fluid Mech., 1998, 358: 61.